Smart Structures and Systems, *Vol. 29, No. 4 (2022) 589-598*
https://doi.org/10.12989/sss.2022.29.4.589

Monitoring moisture content of timber structures using PZT-enabled sensing and machine learning

Lin Chen [a], Haibei Xiong, Yufeng He, Xiuquan Li and Qingzhao Kong*

Department of Disaster Mitigation for Structures, Tongji University, 1239 Siping Road, Shanghai 200092, Republic of China

(*Received September 6, 2021, Revised December 9, 2021, Accepted December 10, 2021*)

Abstract. Timber structures are susceptible to structural damages caused by variations in moisture content (MC), inducing severe durability deterioration and safety issues. Therefore, it is of great significance to detect MC levels in timber structures. Compared to current methods for timber MC detection, which are time-consuming and require bulky equipment deployment, Lead Zirconate Titanate (PZT)-enabled stress wave sensing combined with statistic machine learning classification proposed in this paper show the advantage of the portable device and ease of operation. First, stress wave signals from different MC cases are excited and received by PZT sensors through active sensing. Subsequently, two non-baseline features are extracted from these stress wave signals. Finally, these features are fed to a statistic machine learning classifier (i.e., naïve Bayesian classification) to achieve MC detection of timber structures. Numerical simulations validate the feasibility of PZT-enabled sensing to perceive MC variations. Tests referring to five MC cases are conducted to verify the effectiveness of the proposed method. Results present high accuracy for timber MC detection, showing a great potential to conduct rapid and long-term monitoring of the MC level of timber structures in future field applications.

Keywords: CFD simulation; moisture content; PZT-enabled sensing; statistic machine learning; structural health monitoring; timber structure

1. Introduction

Wood materials have been increasingly utilized in building constructions because of the high environmental friendliness (Chen *et al*. 2020). Due to that wood is a biomass material, timber structures are susceptible to suffer damages caused by environmental variations during the service period. The mechanical properties of timber components exhibit intense temperature and humidity dependency. The variations of MC mainly affect the mechanical properties of timber components (Palma and Steiger 2020). With the increase of MC in timber material, especially when MC exceeds the fiber saturation point, the risk of wood-decaying fungal growth significantly increases, reducing the durability and safety of timber structures (Dietsch *et al*. 2014, Nocetti *et al*. 2015, Walker *et al*. 2016). Many design codes of timber structures have specified the attenuation coefficient of strength design values to consider MC effects (EN 335-1 2006, ISO 3131 1975). Thus, it is of great importance to detect the MC level in timber structures.

Currently, many non-destructive approaches have been proposed to monitor MC levels of timber structures, mainly including the electrical resistance method (Franke *et al*. 2014), ground-penetrating radar (GPR) technique (Halabe *et al*. 2007), X-ray tomography (Couceiro *et al*. 2020), microwave method (Johansson *et al*. 2003), and infrared thermography technique (Kandemir-Yucel *et al*. 2007, Kylili *et al*. 2014). Among these methods, electrical resistance method applies two drilling electrodes to obtain the resistance of a local region of timber and then calculates the MC through the empirical relationship between electrical resistance and MC, which is highly affected by the penetration depth and shows heavy uncertainties when air temperature changes. Other methods based on GPR, X-ray tomography, microwave and infrared thermography show the advantage of contact-free detection. However, most of these methods are very time-consuming and require costly and bulky equipment deployment, causing difficulties in field application (Palma and Steiger 2020). Compared with the methods mentioned above, the stress wave-based method is of great potential for rapid and effective detection of MC level of timber strictures because of the portable device and simple operation.

Conventional stress wave-based detection utilizes ultrasonic probes to excite and receive stress waves and mainly uses the empirical relationship between the MC and wave speed to evaluate the MC level. The propagation of stress waves and the calculated wave speed are highly affected by the boundary coupling agent and insertion angle, which may bring uncertainties to MC estimation results. Furthermore, some smart sensors without the particular coupling agent and operation requirement have gained increasing attention to excite and receive stress waves in detection. Lead Zirconate Titanate (PZT), as one type of smart material with the advantage of small size, low

*Corresponding author, Ph.D., Professor,
E-mail: qkong@tongji.edu.cn
[a] Ph.D., E-mail: 1710742@tongji.edu.cn

ISSN: 1738-1584 (Print), 1738-1991 (Online)

cost, and high environmental-adaptability (Feng *et al*. 2016, Nguyen *et al*. 2013), is widely adopted as sensors in structural health monitoring (SHM) (Xu *et al*. 2018, Yuan *et al*. 2020, Huynh and Kim 2016, Park *et al*. 2005). Zhang *et al*. 2018 first applied PZT sensors to monitor the MC states of timber structures and preliminarily validated the feasibility. In the aforementioned research, a MC indicator was proposed based on the variation of signal energy in different frequency bands. However, the value of this one-dimensional indicator is susceptible to be affected by accidental factors in measurement and highly depends on the selection of baseline signal.

To avoid this issue, some machine learning techniques have been utilized to process stress wave signals and achieve auto-classification or clustering of massive monitoring signals. Mainly used machine learning techniques include K-Nearest Neighbors (K-NN) algorithm (Vitola *et al*. 2017), Support Vector Machine (SVM) learning (Park *et al*. 2006), Hidden Markov model (HMM) (Ebrahimkhanlou *et al*. 2018, Zaidi *et al*. 2011), and Random Forest (RF) algorithm (Yuan *et al*. 2021, Wang *et al*. 2021). Wang and Song 2020 utilized RF classifier and stress wave-based sensing to achieve looseness detection of multi-bolt connections in normal service conditions and underwater environments. HMM and a convolutional neural network has been used to identify fatigue cracks of an aircraft structure based on stress wave signals captured in the loading process (Mei *et al*. 2016, Xu *et al*. 2019). As mentioned above, we can find that machine learning-assisted classification has gained much attention in SHM, while research on MC detection of timber structures using machine learning-assisted stress wave sensing has not been reported yet.

In the present study, the authors proposed a new detection method for MC of timber structures using PZT-enabled sensing combined with statistic machine learning. First, two simple and baseline-free signal features are extracted from stress wave signals which are excited and received by PZT sensors from different MC cases of timber components. And then naïve Bayesian classification is used to classify these signal features. In addition, the generality of the proposed method to detect MC levels when the crack exists was investigated. This paper was organized as follows. Section 2 described the calculation procedure of the proposed method. Section 3 validated the feasibility of using PZT-enabled sensing to perceive the variation of MC values based on numerical simulation. Laboratory tests for different MC cases of timber structures were described in Section 4. Finally, results and discussions were depicted in Section 5, and conclusions were presented in Section 6.

2. Theoretical background

As the flowchart illustrated in Fig. 1, the MC detection method proposed in this paper mainly consists of three steps. Stress wave signals are first captured by PZT sensors from different MC cases. To validate the robustness and generality of the proposed method, two additional specimens with cracks are also tested. Subsequently, wavelet packet decomposition (WPD) is used to reconstruct original stress wave signals to eliminate the crosstalk component. Then, two baseline-free features (i.e., signal energy and the amplitude of peak frequency) are extracted from these preprocessed signals. Finally, features are fed to the naïve Bayesian classifier to realize MC detection.

2.1 Signal reconstruction and features extraction

Signals collected by the data acquisition system are susceptible to the crosstalk phenomenon, causing a large number of low-frequency components and even DC components. To eliminate the effect of these unexpected signals, the authors use the WPD method to reconstruct original stress wave signals. WPD is developed from wavelet transformation (WT), which can decompose a signal into the low-frequency component and high-frequency component. For a discrete collected signal, the WT is calculated as

$$DWT_{j,k} = \langle X(t), \psi_{j,k}(t) \rangle = \sum_{j,k \in Z} X(t)\, \psi_{j,k}(t) dt \quad (1)$$

where $DWT_{j,k}$ is the decomposed signal of the k node in the j layer decomposition, $X(t)$ is the original signal, and $\psi_{j,k}(t)$ is discrete wavelet function.

Many damage features, which are extracted from stress wave signals in the time domain, frequency domain, and time-frequency domain, have been developed in stress wave-based structural health monitoring (Su *et al*. 2009, Zeng *et al*. 2015). Most of these damage features are calculated by comparing the variations between signals collected from damage cases and the health case, namely the baseline signal. However, the baseline signal is often difficult to be obtained in many applications.

In this research, two simple damage features are directly extracted from the stress wave signal to avoid the requirement of the baseline signal. The first damage feature is the signal energy, which is extracted from the time domain, which can be calculated as Eq. (2)

$$E = \int_{t1}^{t2} X^2(t)\, dt \quad (2)$$

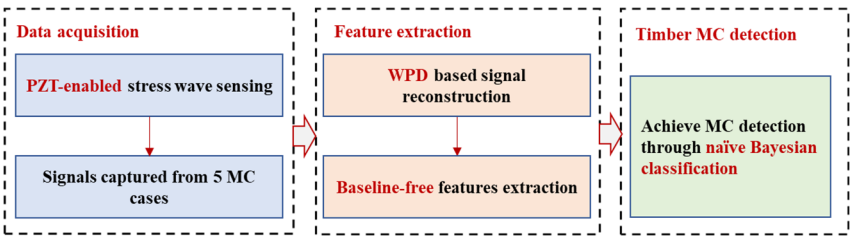

Fig. 1 Flowchart of the proposed method

where E is the signal energy, t_1 and t_2 are the start and stop time of the collected stress wave signal, $X(t)$ is the collected monitoring signal.

The second damage feature is the amplitude of peak frequency, which is extracted from the frequency domain, as defined in follows

$$A = \max_{f_1 \le f \le f_2} (|X(f)|) \tag{3}$$

where $X(f)$ is Fourier transform of the collected stress wave signal, f_1 and f_2 are the start and the stop frequency of monitoring signals in the frequency domain.

2.2 Naïve Bayesian classification

Naïve Bayesian classification is a mainly used probabilistic model of statistical machine learning, which has the advantage of simple implementation and high learning efficiency. For a certain training dataset, naïve Bayesian classification first computes the prior probability distribution based on the statistic of training dataset, and then learns the conditional probability distribution according to the feature condition independent assumption (Liu *et al*. 2011). This assumption is the underlying principle of naïve Bayesian classification, which is described as follows

$$\begin{aligned} P(x|y=c_i) &= P\left(x^{(1)}, x^{(2)}, \cdots, x^{(n)} | y=c_i\right) \\ &= \prod_{j=1}^{n} P(x^{(j)}|y=c_i) \end{aligned} \tag{4}$$

where x represents the n-dimensional eigenvector, $x^{(j)}$ is the j^{th} eigenvalue, y refers to the class label, which belongs to a category set $C = \{c_1, c_2, \cdots, c_K\}$. The number of class label is K.

As Fig. 2 showed, the detailed calculation procedure of naïve Bayesian classification mainly includes two steps. In the step of generating model, a training dataset is used to generate the naïve Bayesian model, it can be expressed as

$$T = \{(x_1, y_1), (x_2, y_2), \cdots, (x_N, y_N)\} \tag{5}$$

where T represents the training dataset, N refers to the number of samples in the training dataset. The variables x and y are the same with Eq. (4).

After calculating the prior probability distribution and conditional probability distribution corresponding to each class label, we obtain the naïve Bayesian model. Then, for a given validation dataset, according to Bayes theorem, the posterior probability referring to a certain class label can be calculated as

$$P(y=c_i|x) = \frac{P(x|y=c_i)P(y=c_i)}{\sum_{i=1}^{K} P(x|y=c_i)P(y=c_i)} \tag{6}$$

Substitute Eq. (4) to Eq. (6), the posterior probability can be expressed as

$$P(y=c_i|x) = \frac{P(y=c_i)\prod_{j=1}^{n} P(x^{(j)}|y=c_i)}{\sum_{i=1}^{K} P(y=c_i)\prod_{j=1}^{n} P(x^{(j)}|y=c_i)} \tag{7}$$

Finally, the prediction label of validation dataset is obtained as the category corresponding to the maximum posterior probability

$$\begin{aligned} y_p &= f(x) \\ &= arg\max_{c_i} \frac{P(y=c_i)\prod_{j=1}^{n} P(x^{(j)}|y=c_i)}{\sum_{i=1}^{K} P(y=c_i)\prod_{j=1}^{n} P(x^{(j)}|y=c_i)} \end{aligned} \tag{8}$$

where y_p is the prediction label.

3. Numerical verification of PZT-enabled sensing

To validate the feasibility of PZT-enabled sensing to perceive the variations of MC of timber material, numerical simulations are conducted in this section.

3.1 Finite element model configuration

The variations of MC mainly affect the density and elastic modulus of timber material. In numerical simulations, we use a series of different material properties to represent different MC cases. Much research has shown that when the moisture content is below the fiber saturation level, elastic modulus and strength of timber decrease with the increase of MC (Kurz and Boller 2015, Ruangkhasap *et al*. 2020, Thelandersson and Larsen 2003). The relationship between elastic modulus, density and MC can be expressed as follows

$$E_{12} = E_{\text{test}} \times \left(1 + \alpha(L_{\text{test}} - 12)\right) \tag{9}$$

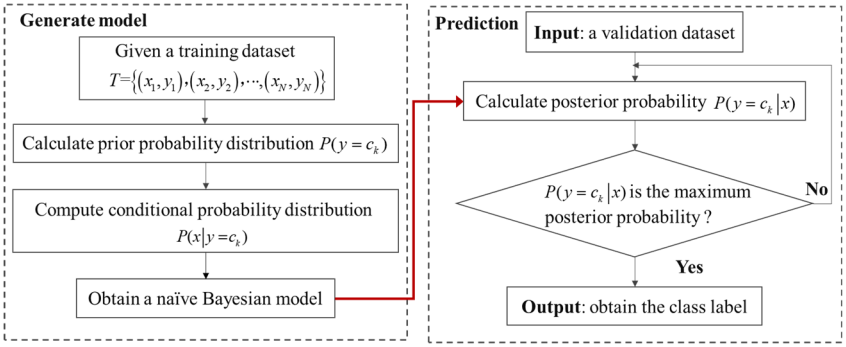

Fig. 2 Calculation procedure of naïve Bayesian classification

Table 1 Mechanical properties at different moisture content levels in simulations

MC (%)	Density (kg/m^3)	Engineering constants (GPa)						Poisson's ratio		
		E_L	E_R	E_T	G_{LR}	G_{LT}	G_{TR}	μ_{LR}	μ_{LT}	μ_{RT}
0	561.90	18.636	2.889	2.000	1.686	1.300	0.113	0.61	0.53	0.90
5	575.61	17.447	1.793	1.241	1.388	1.070	0.093	0.51	0.44	0.74
10	590.00	16.400	1.300	0.900	1.180	0.910	0.079	0.43	0.37	0.63
15	605.13	15.472	1.019	0.706	1.026	0.791	0.069	0.37	0.32	0.55
20	621.05	14.643	0.839	0.581	0.908	0.700	0.061	0.33	0.28	0.48

*Note: L refers to the longitudinal direction, R represents the radial direction, and T refers to the tangential direction

Table 2 Mechanical properties of PZT used in simulations

Engineering constants (GPa)		Piezoelectric coupling matrix (m/volt) × E – 10	
$E1$	60.61	$d311$	-2.74
$E2$	60.61	$d322$	-2.74
$E3$	48.31	$d333$	5.93
$v12$	0.289	$d112$	7.41
$v13$	0.512	$d223$	7.41
$v23$	0.512	Dielectric matrix (farad/meter) × E – 08	
$G12$	23.5	$D11$	1.505
$G13$	23	$D22$	1.505
$G23$	23	$D33$	1.301

*Note: direction 1 refers to length direction, direction 2 is the width direction, and direction 3 represents the thickness direction of the PZT patch

$$\rho_{12} = \rho_{\text{test}} \times \left(1 - 0.01 \times (1 - \beta) \times (L_{\text{test}} - 12)\right) \quad (10)$$

where E_{12} is the elastic modulus at the equilibrium moisture content (EMC), E_{test} refers to the elastic modulus at the MC of L_{test}, and α is the scale factor, as for elastic modulus, α can be taken as 0.012. ρ_{12} is the density at 12% moisture content, ρ_{test} refers to the density at a MC of L_{test}, β is the volume contracts coefficient, which is set as 0.50 in this research.

Take a set of mechanical properties of timber as a reference. The mechanical properties of five cases that refer to different MC are listed in Table 1. And the mechanical property of PZT patches is listed in Table 2.

3.2 Simulation analysis

After defining mechanical properties, a series of finite element models (FEM) corresponding to different mechanical properties are established. The dimension of the FEM is 300 mm in length, 100 mm in width, and 50 mm in height. Additionally, the size of PZT patches is 10 mm in length and width, and 2 mm in height. The Dynamic Implicit solver is used, and the step time is set as 0.001 sec. A Hanning window modulated sine wave is applied as the excitation electric potential of PZT patches. The boundary of PZT patches and timber structure is set as the Tie interface. After meshing, a total of 23408 elements are obtained. As Fig. 3 showed, the element type of PZT is set as C3D8E which has the piezoelectric effect, and timber specimen is set as C3D8R. The excitation signal of PZT elements is described in Fig. 4. The amplitude of excitation

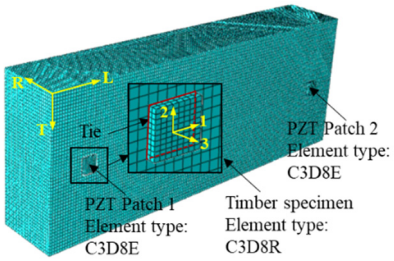

Fig. 3 Mesh information of FEM

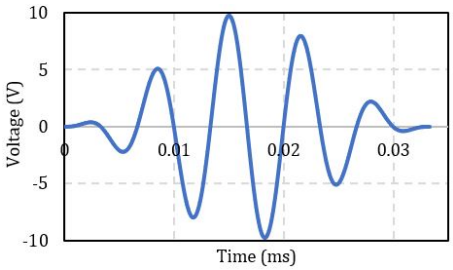

Fig. 4 Excitation signal

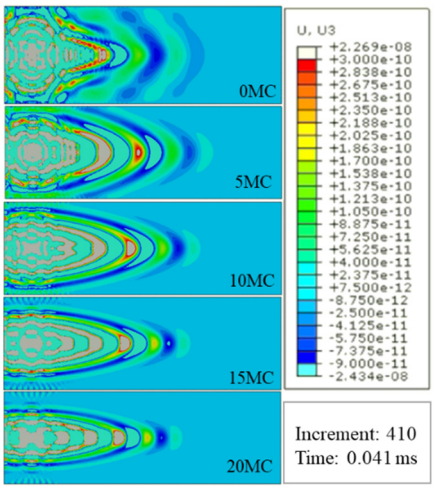

Fig. 5 Contours of displacement in MC cases

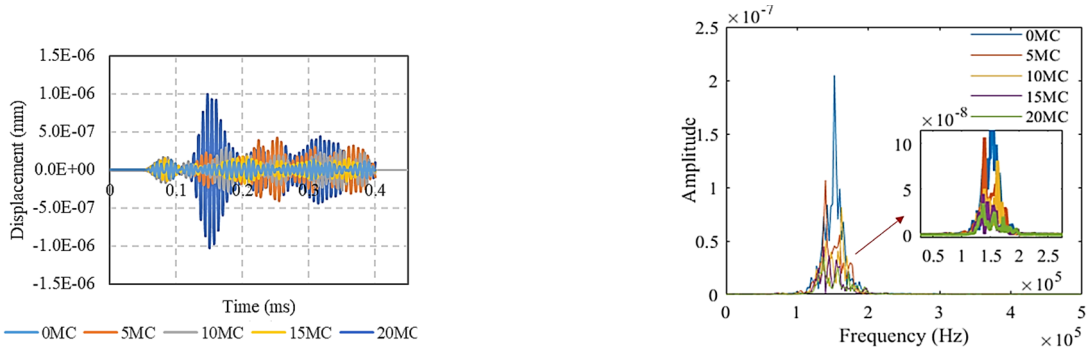

(a) Time domain (b) Frequency domain

Fig. 6 Received signals of FEM

signal is 10 V, and the duration is 3.33E-2 ms. Note that only one PZT patch 1 is excited.

The simulation results of five MC cases are shown in Fig. 5. The selected surface of timber specimen is the PZT-installed surface. In the same step time, with the increase of MC, the displacement contours of the timber specimen show significant variations, displaying the reduction of propagation velocity in the width direction.

Fig. 6 shows received signals of FEM. The selected node is on the timber specimen, which position is corresponding to the center of bottom surface of PZT patch 2. As Fig. 6 showed, the received signal performs large variations with different MC in both time and frequency domain. In the time domain, the most obvious change is the amplitude, which affects the signal energy. In the frequency domain, the amplitude of peak frequency shows significant variations. The simulation results validate the feasibility of using PZT-enabled sensing to perceive MC variations and further implies the signal energy in time domain and the amplitude of peak frequency in frequency can be the indicator to reflect MC variations.

4. Experimental setup

4.1 Test specimen

Timber specimen (pine wood) with different moisture contents was prepared at the laboratory. The dimension of timber specimens is 300 mm × 100 mm × 50 mm. Relative moisture content (0% assumed at room temperature and humidity) was adopted, which varied from 0% to 20% with 5% increments. Timber specimens were soaked in the water with different time to obtain different masses corresponding to designed MC cases. To eliminate the effect of water on PZT sensors, epoxy adhesive is used to wrap PZT patches. Certain MC was controlled by measuring the mass of timber specimens (Eq. (11)) using an electronic scale. The mass of timber specimens in wet conditions was determined when the two adjacent measurements are the same. An absolute error between the designed MC level and the measured MC within 1% can be accepted in the test. The measuring recording is listed in Table 3. To investigate the generality of the proposed method to detect MC of timber when timber specimens have the surface crack, two timber specimens with the same size were pre-cut different depth cracks and also tested.

$$MC = \frac{m_{\text{wet}} - m_{\text{dry}}}{m_{\text{dry}}} \times 100\% \tag{11}$$

where MC represents to the moisture content, m_{wet} is the mass of timber in wet condition, and m_{dry} represents the mass of timber in dry condition.

4.2 Data acquisition

Fig. 7 shows three specimens in relative 0% MC and soaking process, and the mainly experimental apparatus which include a data-acquisition system, a power amplifier (Trek Model 2100HF) and a monitoring terminal. After soaking for a period of time, timber specimens will be taken out and weigh the mass. If the mass of specimen near the corresponding designed MC cases, then we conduct the stress wave test. Two PZT patches (one as actuator and another as sensor) were mounted on the top surface of timber specimens to excite and receive stress waves. The authors adopted adhesive (Comix super glue B2695) to fix

Table 3 Recording of the measured mass for different MC cases

No. specimen	Crack depth (mm)	Initial mass (g)	Mass in designed relative MC cases (g)							
			5%		10%		15%		20%	
			Mass	Error	Mass	Error	Mass	Error	Mass	Error
S1	0	654.0	690.9	0.64%	723.0	0.55%	754.7	0.40%	788.7	0.60%
S2	4	643.0	680.0	0.75%	712.0	0.73%	745.2	0.89%	777.3	0.89%
S3	8	647.0	683.5	0.64%	716.4	0.73%	749.0	0.77%	780.9	0.70%

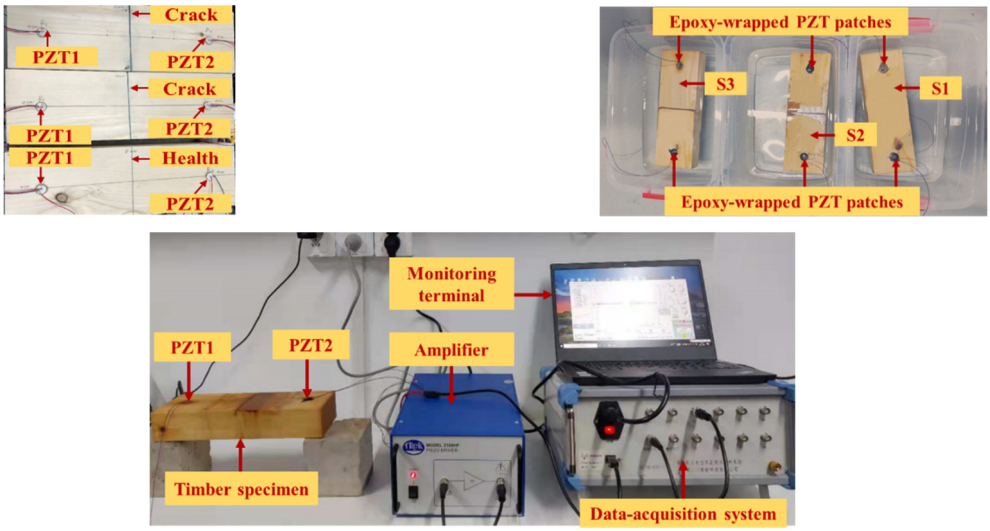

Fig. 7 Specimen preparation and experimental apparatus

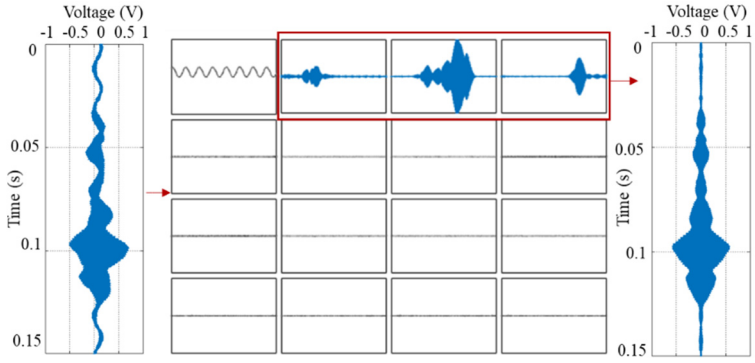

Fig. 8 Wavelet packet decomposition and reconstruction

sensors on the predetermined location, and then used the epoxy resin to enclose the PZT transducers. The epoxy resin provides a waterproof function when specimens are immersed in water. A linear swept wave (frequency range: 50-300 kHz, amplitude: 10 V, duration: 0.25 sec) was adopted since no prior knowledge of the specimen is needed, and it was generated by the monitoring terminal. For each case, the authors repeated the stress wave test ten times.

5. Results and discussion

5.1 Signal preprocessing

Following the test procedure described in Section 4, a total of 50 stress wave signals were obtained after tests. Due to the power-line interference, raw data was aliased with a low-frequency sine wave. Thus, WPD based reconstruction is conducted on the raw data to eliminate undesirable frequency band signals. Four-layer WPD is adopted in this research, and a total of 16 sub-frequency signals are obtained. Fig. 8 shows the reconstruction procedure of the raw data. Note that the range of the vertical axis is the same with decomposed signals. The sampling frequency is 2000 kHz. According to the Nyquist sampling theorem, the maximum frequency of decomposed signals is 1000 kHz. Thus, the frequency range of the first sub-frequency signal is 0 Hz to 62.5 kHz, and the increment of two adjacent sub-signals is 62.5 kHz. It is clear that the first frequency band is the power-line interference. The 2nd, 3rd, and 4th frequency band signals contribute nearly all parts of the original raw data, which are used to reconstruct signals.

Fig. 9 depicts the received stress wave signals and their corresponding signal energy and Fourier spectrums of three specimens after preprocessing. Several peaks can be observed in each received signal because reflection and scattering waves arrived at PZT sensor at different moments. With the increase of MC, raw signals and frequency spectrums show obvious variations. Signals of 20% MC have the smallest energy in these three specimens, while signal energies do not perform monotonous statistical variations over the increasing MC. Thus, the conventional classification method based on damage index will not be applicable.

5.2 Features distribution

As mentioned above, we repeat ten times in each test case. Thus, a total of 50 signals for each specimen are obtained. Due to that the number of signals is a little small for machine learning, data augmentation is conducted on

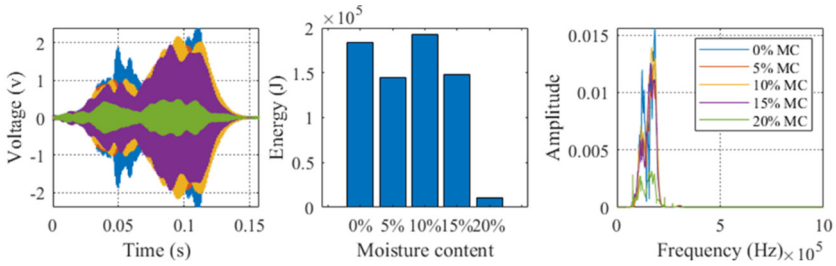

(a) Specimen 1

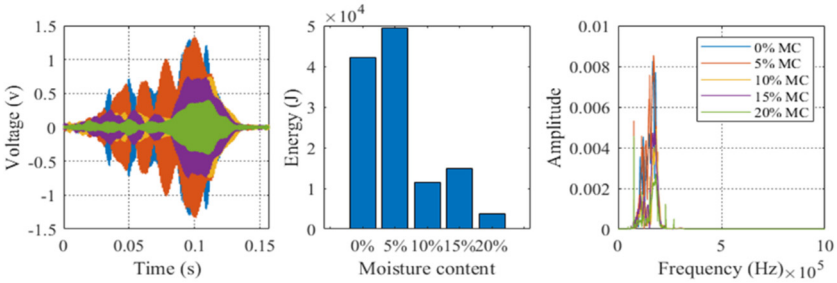

(b) Specimen 2

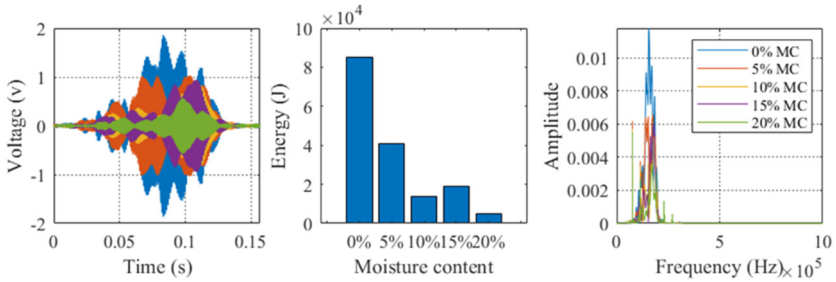

(c) Specimen 3

Fig. 9 Stress wave signals after preprocessing

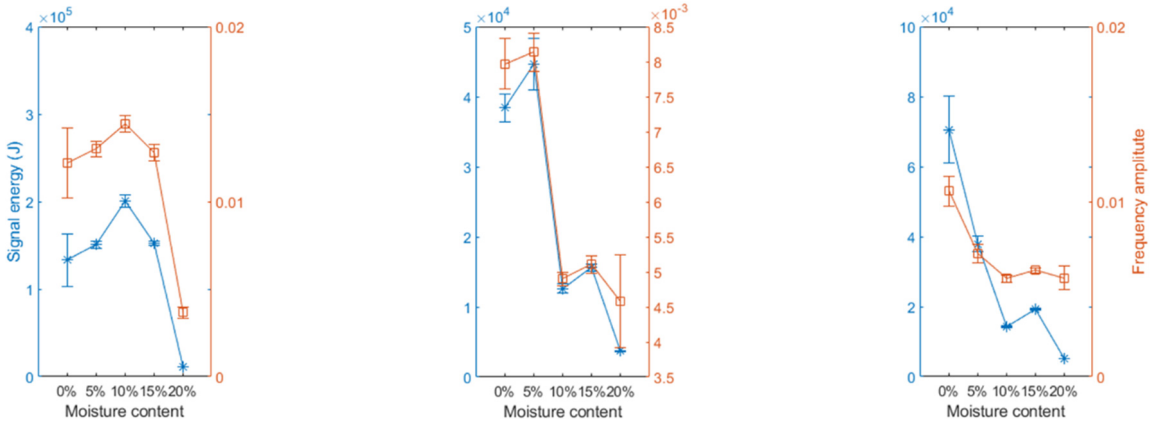

(a) Specimen 1 (b) Specimen 2 (c) Specimen 3

Fig. 10 Energy and frequency amplitude of received signals under different moisture content

the raw data to expand the dataset. A series of white Gaussian noises are added into each raw data with a random signal-to-noise ratio (SNR) in the range of 15 dB and 45 dB. After data augmentation, 250 signals in each specimen are obtained. Then, energy and the amplitude of peak frequency are extracted and consist of the eigenvector to conduct naïve Bayes classification further. Fig. 10 shows the distribution of extracted features. With the increase of MC, the variation of energy and the amplitude of peak frequency shows uncertainties and large variance.

5.3 Classification results

Signal energy and the amplitude of peak frequency are raw data features, and their corresponding MC are set as labels. We repeat five times in each specimen to validate the

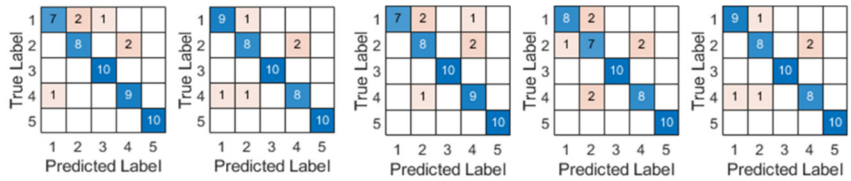

(a) Specimen 1

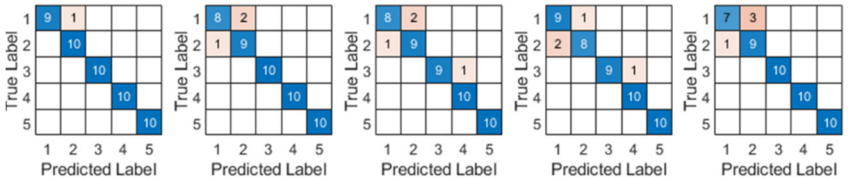

(b) Specimen 2

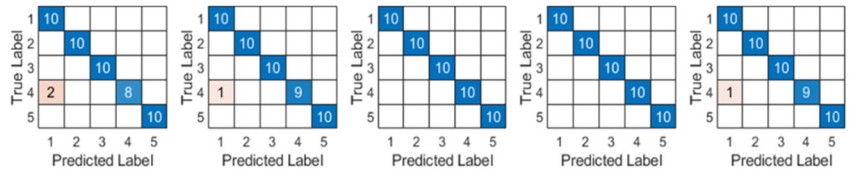

(C) Specimen 3

Fig. 11 Confusion matrix over 5 times

stability of the trained model. In each training time, 80% of samples of each class are randomly split as training set and the rest of 20% samples are set as the validation set, which means a different model will be trained in each training time. Since samples in each class are repeatedly sampled and then added random white Gaussian noise, the normal distribution is adopted for predictors (i.e., signal energy and the amplitude of peak frequency). Then, the naive Bayes classifier estimates a separate normal distribution for each class by computing the mean and standard deviation of the training data in that class. Fig. 11 gives the prediction results of each specimen over five times. The number of wrong predictions in specimen 1 is in the range of 5 to 7, 1 to 4 for specimen 2, and 0 to 2 for specimen 3, displaying a descending trend from specimen 1 to specimen 3. Fig. 12 summarizes the prediction accuracy of three specimens over five times. It is clear that the proposed method shows high prediction accuracy and generality to identify the variation of MC despite cracks existing.

5.4 Discussions and future work

Test results of this study have shown the effectiveness of the proposed method to detect MC condition of timber structures. However, some issues would impede the practical applications of using PZT-enabled sensor and statistic machine learning to monitor MC levels in timber engineering. The first issue is the integration of sensors and structures. Surface-mounted PZT sensors used in this research would change the appearance of structures and are susceptible to variations of environments. One preliminary solution of future work is to design an implantable module which can be assembled with timber components in factory to realize the integration of sensors and structures. The second issue is the propagation distance of PZT-enabled sensing. Due to that real structure components have larger size and stress wave shows relatively high dispersive characteristic in timber material, the enhancement of signals is needed. One possible solution is to deploy an amplifying

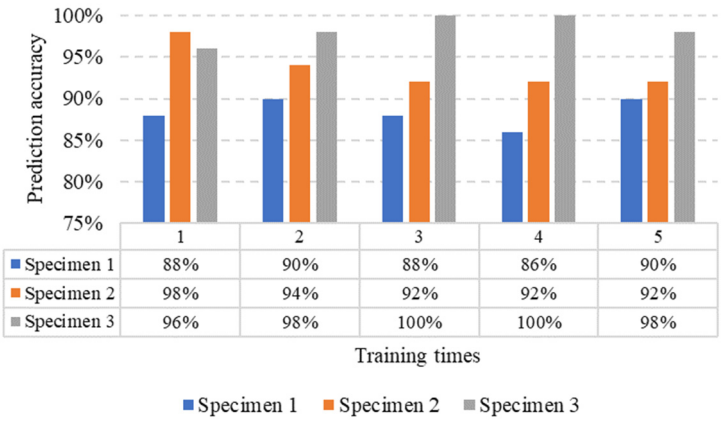

Fig. 12 Prediction accuracy of three specimens

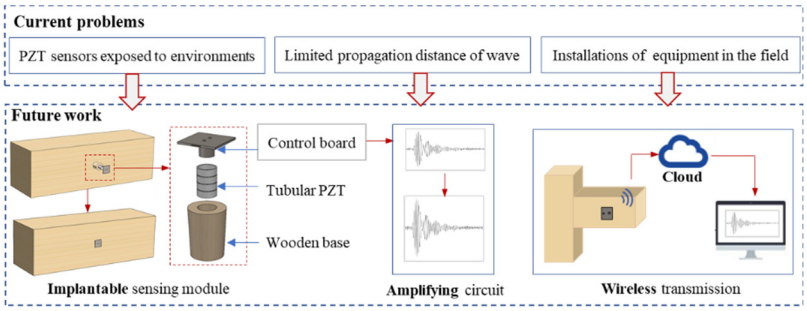

Fig. 13 The framework of future work

circuit in the receiving end of sensors. The third issue is the configuration of monitoring system. To avoid bulky wire and equipment in the field of each project, wireless sensors and signal transmission would be studied in future work. The framework of future work as the consideration of solving the challenging issues of the proposed method in field applications is shown in Fig. 13.

6. Conclusions

In this research, the authors propose a detection method for MC level in timber structures using PZT-enabled stress wave sensing combined with statistic machine learning classification. Compared with traditional MC detection methods, the proposed method shows the advantage of the portable device and ease of operation, which has great potential to apply in real engineering projects. Compared with current stress wave-based method, the features used in this paper are directly extracted from each stress wave signal, which is baseline-free and thus has larger generality in applications. These features are fed to the naïve Bayesian classifier to realize the detection of MC levels of timber structures. Numerical simulation validates the feasibility of PZT-enabled stress wave sensing to perceive the MC variations. Experimental results demonstrate that the MC level of timber structures can be detected through the proposed method with high accuracy despite the effect of the existing crack.

Acknowledgments

The authors greatly appreciate the financial support of the National Natural Science Foundation of China (Grant number 52020105005; 51978502) and the Science and Technology Commission of Shanghai Municipality (Grant number 20692114200; 19DZ1202502).

References

Chen, J., Xiong, H., Wang, Z. and Yang, L. (2020), "Experimental buckling performance of eucalyptus-based oriented oblique laminated strand lumber columns under centric and eccentric compression", *Constr. Build. Mater.*, **262**, 120072. https://doi.org/10.1016/j.conbuildmat.2020.120072

Chen, L., Xiong, H., Sang, X., Yuan, C. and Kong, Q. (2021), "An innovative deep neural network–based approach for internal cavity detection of timber columns using percussion sound", *Struct. Health Monitor.*, 147592172110285. https://doi.org/10.1177/14759217211028524

Couceiro, J., Hansson, L., Sehlstedt-Persson, M., Vikberg, T. and Sandberg, D. (2020), "The conditioning regime in industrial drying of Scots pine sawn timber studied by X-ray computed tomography: a case-study", *Eur. J. Wood Wood Prod.*, **78**(4), 673-682. https://doi.org/10.1007/s00107-020-01549-2

Dietsch, P., Franke, S., Franke, B., Gamper, A. and Winter, S. (2014), "Methods to determine wood moisture content and their applicability in monitoring concepts", *J. Civil Struct. Health Monitor.*, **5**, 115-127. https://doi.org/10.1007/s13349-014-0082-7

Ebrahimkhanlou, A., Choi, J., Hrynyk, T.D., Salamone, S. and Bayrak, O. (2018), "Detection of the onset of delamination in a post-tensioned curved concrete structure using hidden Markov modeling of acoustic emissions", *Proceedings of Sensors and Smart Structures Technologies for Civil, Mechanical, and Aerospace Systems 2018*, Denver, CO, USA, March. https://doi.org/10.1117/12.2296624

EN 335-1 (2006), Durability of Wood and Wood-Based Products–Definition of use classes–Part 1: General.

Feng, Q., Kong, Q. and Song, G. (2016), "Damage detection of concrete piles subject to typical damage types based on stress wave measurement using embedded smart aggregates transducers", *Measurement*, 345-352. https://doi.org/10.1016/j.measurement.2016.01.042

Franke, B., Franke, S. and Müller, A. (2014), "Case studies: long-term monitoring of timber bridges", *J. Civil Struct. Health Monitor.*, **5**(2), 195-202. https://doi.org/10.1007/s13349-014-0093-4

Halabe, U., Agrawal, S., Gopalakrishnan, B. and Grushecky, S. (2007), "Defect detection in wooden logs using ground penetrating radar", **894**, 1368-1375. https://doi.org/10.1063/1.2718125

Huynh, T.-C. and Kim, J.-T. (2016), "Compensation of temperature effect on impedance responses of PZT interface for prestress-loss monitoring in PSC girders", *Smart Struct. Syst., Int. J.*, **17**(6), 881-901. https://doi.org/10.12989/sss.2016.17.6.881

ISO 3131 (1975), Wood-Determination of density for physical and mechanical tests.

Johansson, J., Hagman, O. and Oja, J. (2003), "Predicting moisture content and density of Scots pine by microwave scanning of sawn timber", *Comput. Electron. Agricult.*, **41**(1), 85-90. https://doi.org/10.1016/S0168-1699(03)00044-9

Kandemir-Yucel, A., Tavukcuoglu, A. and Caner-Saltik, E.N. (2007), "In situ assessment of structural timber elements of a historic building by infrared thermography and ultrasonic velocity", *Infrared Phys. Technol.*, **49**(3), 243-248. https://doi.org/10.1016/j.infrared.2006.06.012

Kurz, J.H. and Boller, C. (2015), "Some background of monitoring and NDT also useful for timber structures", *J. Civil Struct. Health Monitor.*, **5**(2), 99-106.

https://doi.org/10.1007/s13349-015-0105-z
Kylili, A., Fokaides, P.A., Christou, P. and Kalogirou, S.A. (2014), "Infrared thermography (IRT) applications for building diagnostics: A review", *Appl. Energy*, **134**, 531-549. https://doi.org/10.1016/j.apenergy.2014.08.005
Liu, J.N., He, Y.L., Wang, X.Z. and Hu, Y.X. (2011), "A comparative study among different kernel functions in flexible naïve Bayesian classification", *Proceedings of 2011 International Conference on Machine Learning and Cybernetics*, Guilin, China, July.
Mei, H., Yuan, S., Qiu, L. and Zhang, J. (2016), "Damage evaluation by a guided wave-hidden Markov model based method", *Smart Mater. Struct.*, **25**(2), 025021. https://doi.org/10.1088/0964-1726/25/2/025021
Nguyen, K.-D., Ho, D.-D. and Kim, J.-T. (2013), "Damage detection in beam-type structures via PZT's dual piezoelectric responses", *Smart Struct. Syst., Int. J.*, **11**(2), 217-240. https://doi.org/10.12989/sss.2013.11.2.217
Nocetti, M., Brunetti, M. and Bacher, M. (2015), "Effect of moisture content on the flexural properties and dynamic modulus of elasticity of dimension chestnut timber", *Eur. J. Wood Wood Prod.*, **73**(1), 51-60. https://doi.org/10.1007/s00107-014-0861-1
Palma, P. and Steiger, R. (2020), "Structural health monitoring of timber structures – Review of available methods and case studies", *Constr. Build. Mater.*, **248**, 118528. https://doi.org/10.1016/j.conbuildmat.2020.118528
Park, S., Yun, C.B., Roh, Y. and Lee, J.J. (2005), "Health monitoring of steel structures using impedance of thickness modes at PZT patches", *Smart Struct. Syst., Int. J.*, **1**(4), 339-353. https://doi.org/10.12989/sss.2005.1.4.339
Park, S., Yun, C.B., Roh, Y. and Lee, J.J. (2006), "PZT-based active damage detection techniques for steel bridge components", *Smart Mater. Struct.*, **15**(4), 957-966. https://doi.org/10.1088/0964-1726/15/4/009
Park, S., Lee, J.J., Yun, C.B. and Inman, D.J. (2007), "Abuilt-in active sensing system-based structural health monitoring technique using statistical pattern recognition", *J. Mech. Sci. Technol.*, **21**(6), 896-902. https://doi.org/10.1007/BF03027065
Ruangkhasap, S., Noypitak, S., Noknoi, W. and Terdwongworakul, A. (2020), "Non-destructive assessment of moisture content and modulus of rupture of sawn timber Hevea wood using near infrared spectroscopy technique", *Proceedings of IOP Conference Series: Materials Science and Engineering*, **773**, 012065. https://doi.org/10.1088/1757-899X/773/1/012065
Su, Z., Wang, X., Cheng, L., Yu, L. and Chen, Z. (2009), "On selection of data fusion schemes for structural damage evaluation", *Struct. Health Monitor.*, **8**(3), 223-241. https://doi.org/10.1177/1475921708102140
Thelandersson, S. and Larsen, H.J. (2003), *Timber Engineering*, John Wiley & Sons, NJ, USA.
Vitola, J., Pozo, F., Tibaduiza, D.A. and Anaya, M. (2017), "A sensor data fusion system based on k-nearest neighbor pattern classification for structural health monitoring applications", *Sensors*, **17**(2), 417. https://doi.org/10.3390/s17020417
Walker, R., Pavia, S. and Dalton, M. (2016), "Measurement of moisture content in solid brick walls using timber dowel", *Mater. Struct.*, **49**(7), 2549-2561. https://doi.org/10.1617/s11527-015-0667-6
Wang, F. and Song, G. (2020), "Monitoring of multi-bolt connection looseness using a novel vibro-acoustic method", *Nonlinear Dyn.*, 1-12. https://doi.org/10.1007/s11071-020-05508-7
Wang, F., Chen, Z. and Song, G. (2021), "Smart crawfish: A concept of underwater multi-bolt looseness identification using entropy-enhanced active sensing and ensemble learning", *Mech. Syst. Signal Process.*, **149**, 107186. https://doi.org/10.1016/j.ymssp.2020.107186
Xu, B., Chen, H., Mo, Y.L. and Zhou, T. (2018), "Dominance of debonding defect of CFST on PZT sensor response considering the meso-scale structure of concrete with multi-scale simulation", *Mech. Syst. Signal Process.*, **107**, 515-528. https://doi.org/10.1016/j.ymssp.2018.01.041
Xu, L., Yuan, S., Chen, J. and Ren, Y. (2019), "Guided wave-convolutional neural network based fatigue crack diagnosis of aircraft structures", *Sensors*, **19**(16), 3567. https://doi.org/10.3390/s19163567
Yuan, C., Kong, Q., Chen, W., Jiang, J. and Hao, H. (2020), "Interfacial debonding detection in externally bonded bfrp reinforced concrete using stress wave-based sensing approach", *Smart Mater. Struct.*, **29**(3), 035039. https://doi.org/10.1088/1361-665X/ab7111
Yuan, C., Zhang, J., Chen, L., Xu, J. and Kong, Q. (2021), "Timber moisture detection using wavelet packet decomposition and convolutional neural network", *Smart Mater. Struct.*, **30**(3), 035022. https://doi.org/10.1088/1361-665X/abdc08
Zaidi, S., Aviyente, S., Salman, M., Shin, K.K. and Strangas, E.G. (2011), "Prognosis of Gear Failures in DC Starter Motors Using Hidden Markov Models", *IEEE Trans. Ind. Electron.*, **58**(5), 1695-1706. https://doi.org/10.1109/TIE.2010.2052540
Zeng, L., Parvasi, S.M., Kong, Q., Huo, L., Li, M. and Song, G. (2015), "Bond slip detection of concrete-encased composite structure using shear wave based active sensing approach", *Smart Mater. Struct.*, **24**(12), 125026. https://doi.org/10.1088/0964-1726/24/12/125026
Zhang, J., Li, Y., Huang, Y., Jiang, J. and Ho, S.-C.M. (2018), "A feasibility study on timber moisture monitoring using piezoceramic transducer-enabled active sensing", *Sensors*, **18**(9), 3100. https://doi.org/10.3390/s18093100

BS